JACS
JOURNAL OF THE AMERICAN CHEMICAL SOCIETY

Communication

pubs.acs.org/JACS

Unique Excavated Rhombic Dodecahedral $PtCu_3$ Alloy Nanocrystals Constructed with Ultrathin Nanosheets of High-Energy {110} Facets

Yanyan Jia, Yaqi Jiang,* Jiawei Zhang, Lei Zhang, Qiaoli Chen, Zhaoxiong Xie,* and Lansun Zheng

State Key Laboratory of Physical Chemistry of Solid Surfaces and Department of Chemistry, College of Chemistry and Chemical Engineering, Xiamen University, Xiamen 361005, China

Supporting Information

ABSTRACT: Ultrathin crystalline nanosheets give an extremely high surface area of a specific crystal facet with unique physical and chemical properties compared with normal three-dimensionally polyhedral nanocrystals (NCs). However, the ultrathin metal nanosheets tend to curl themselves or assemble with each other sheet by sheet, which may reduce the effective surface area and accordingly the catalytic activity to a great extent. Here we report a facile wet-chemical route that allows the fabrication of novel excavated rhombic dodecahedral (ERD) $PtCu_3$ alloy NCs with ultrathin nanosheets of high-energy {110} facets. The surface area was measured to be 77 m^2 g^{-1} by CO stripping, although the particle size is about 50 nm. Electrochemical characterizations showed that the ERD $PtCu_3$ NCs exhibit excellent electrocatalytic performance and high antipoisoning activity in comparison with commercial Pt black and $PtCu_3$ alloy NCs with {111} surfaces.

Noble-metal Pt nanocrystals (NCs) are the most promising catalysts in a wide range of application fields.[1] Considering its expensive price and limited availability, there is an urgent need to reduce its overall use. Embedding non-noble-metal atoms into the pure Pt lattice to form Pt-based alloy catalysts has been demonstrated to be an effective way to reduce the usage amount of Pt. More importantly, it has been found that the catalytic activity of Pt-based alloy NCs can be considerably enhanced by modulation of the electronic structure resulting from the alloy structure.[2] Besides the composition, it is well-known that the catalytic property of metal NCs also has a close relationship to their surface structure, which is determined by the shape to a large extent.[3] Tremendous efforts have been made to synthesize bimetallic NCs with different morphologies in order to regulate their surface structure. The majority of Pt-based alloy NCs prepared to date are convex polyhedra such as cubes, octahedra, and tetrahedra enclosed by low-index faces with low surface energy.[4] Those high-energy surfaces with a high density of low-coordinated atoms usually have high catalytic activity toward specific reactions. However, because of the minimization of total surface energy, developing and preserving high-energy surfaces during growth of NCs is difficult and remains a great challenge.[5] On the other hand, ultrathin crystalline metal nanosheets give an extremely high surface area of a specific crystal facet with unique physical and chemical properties compared with normal three-dimensionally polyhedral nanocrystals. However, the ultrathin metal nanosheets tend to curl themselves or assemble with each other sheet by sheet, which may reduce the effective surface area and accordingly the catalytic activity to a great extent. The excavated or concave structure possesses a much larger surface to volume ratio than the convex one and can prevent NCs from aggregating, which would greatly benefit retention of the effective activities during practical applications. Therefore, the excavated polyhedral structure with high-energy surfaces is highly desired to improve the physical and chemical properties of the NCs.[6] Here we report a facile synthetic strategy for preparing unique excavated rhombic dodecahedral (ERD) $PtCu_3$ alloy NCs constructed of 24 ultrathin nanosheets with high-energy {110} facets by coreduction of the metal precursors $Pt(acac)_2$ and $Cu(acac)_2$ with *n*-butylamine as a surface regulator. The as-prepared ERD $PtCu_3$ NCs have a very large surface area and display excellent catalytic activity and antipoisoning ability in the electrocatalytic oxidation of formic acid.

Figure 1a shows a representative scanning electron microscopy (SEM) image of the unique ERD $PtCu_3$ NCs prepared via wet-chemical reduction of $Pt(acac)_2$ and $Cu(acac)_2$ using *N*,*N*-dimethylformamide (DMF) as both the solvent and a weak reductant in the presence of *n*-butylamine and cetyltrimethylammonium chloride (CTAC). These NCs are comparatively uniform with an average size of 50 nm. The powder X-ray diffraction (XRD) pattern of the as-prepared sample (Figure 1b) matches well with that of the standard $PtCu_3$ alloy (JCPDS no. 035-1358), where all of the peaks can be indexed to a face-centered cubic (fcc) structure with cell parameter $a = 3.706(1)$ Å. The composition of the pure-phase $PtCu_3$ alloy was further confirmed by elemental analysis using inductively coupled plasma atomic emission spectrometry (ICP-AES), by which the Cu content in the sample was measured to be 75.05 atom %. In addition, high-angle annular dark-field scanning transmission electron microscopy/energy-dispersive X-ray spectroscopy (HAADF-STEM-EDS) mapping was used to analyze the distribution of Pt and Cu in the NCs. The HAADF-STEM-EDS elemental mapping analysis showed that the distribution ranges of Pt and Cu completely overlapped (Figure 1c), further confirming the as-prepared sample to be a $PtCu_3$ alloy. To certify the shape of the as-prepared $PtCu_3$ NCs, magnified SEM and transmission electron microscopy (TEM) images of individual NCs were carefully observed (Figure 1d,e). Although the outline of each nanocrystal seems to be different, the as-prepared NCs actually have a uniform ERD shape consisting of 24 ultrathin

Received: December 29, 2013
Published: February 28, 2014

dx.doi.org/10.1021/ja413209q | J. Am. Chem. Soc. 2014, 136, 3748−3751

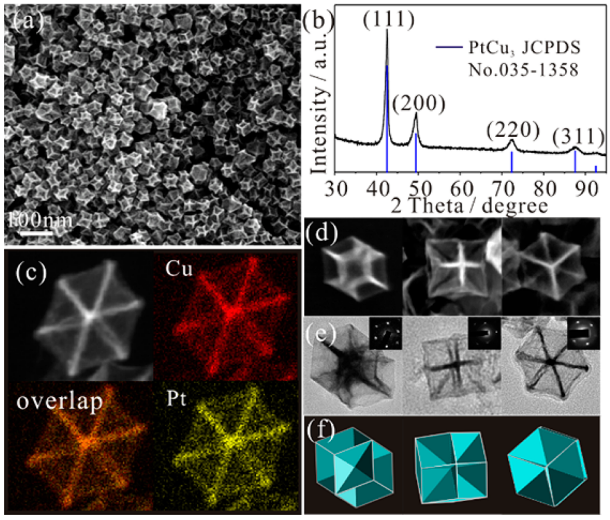

Figure 1. (a) SEM image of the ERD $PtCu_3$ NCs on a large scale. (b) XRD pattern of the ERD $PtCu_3$ alloy NCs. (c) HAADF-STEM image and HAADF-STEM-EDS maps of a single ERD $PtCu_3$ alloy nanoparticle. (d) SEM images and (e) High-magnification TEM images and (insets) the corresponding SAED patterns of an individual ERD $PtCu_3$ alloy NC with different orientations. (f) Schematic models of an ERD $PtCu_3$ alloy NC viewed along the [110], [100], and [111] directions.

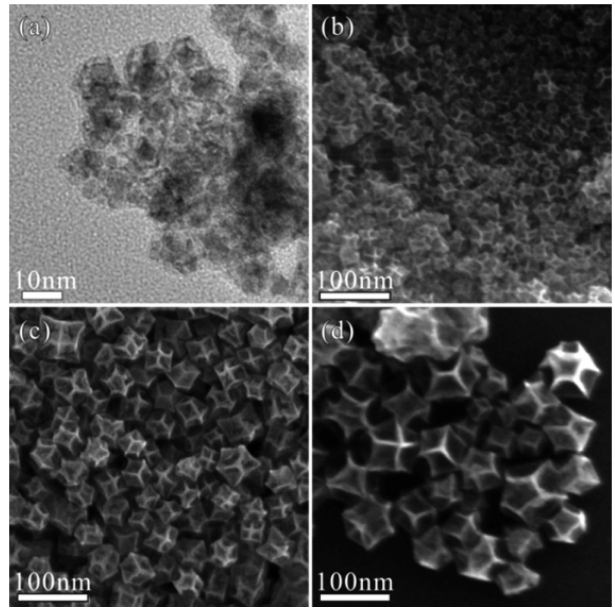

Figure 2. (a) TEM and (b–d) SEM images of the ERD $PtCu_3$ NCs formed at different reaction times: 1.5, 3, 10, and 20 h, respectively.

nanosheets of {110} surfaces with different orientations [also see Figure S1 in the Supporting Information (SI)]. Figure 1f shows typical schematic models of such an ERD nanocrystal projected along the [110], [100], and [111] directions of an fcc lattice that which match well with the corresponding SEM and TEM images in Figure 1d,e. In addition to the SEM and TEM observations, the HAADF-STEM image (Figure 1c, top left), which directly reflects the spatial density of the material, unambiguously demonstrates the ERD structure of the as-prepared NCs, where the bright area corresponds to the vertically oriented nanosheets and the less bright area to the tilted nanosheets. From TEM images of different tilting angles of an individual excavated nanoparticle (Figure S2), the thickness of the ultrathin nanosheets was determined to be approximately 2 nm. In one word, the above structural analyses confirm that the as-prepared $PtCu_3$ NCs take the shape of fully excavated rhombic dodecahedra constructed from 2 nm thick nanosheets. Such fully excavated polyhedral structures have a significantly larger surface area with a theoretical value of about 82 $m^2\ g^{-1}$. The active surface area was measured to be 58 $m^2\ g^{-1}$ by hydrogen desorption and 77 $m^2\ g^{-1}$ by CO stripping. The surface area determined by CO stripping closer to the theoretical value, which was also found for some other Pt–transition metal alloys.[1e]

From a crystallographic point of view, the formation of an excavated polyhedron is very unusual, as the formation of convex polyhedra should be preferred during crystallization because of the minimization of the total surface energy. Thus, a series of experiments were designed and carried out to get a deeper insight into how the ERD structure developed. We first studied the shape evolution with reaction time. The intermediate products at different reaction times were observed by TEM, SEM, and XRD (Figure 2 and Figure S3), which showed that the ERD $PtCu_3$ NCs were formed at the early stage. After 1.5 h of reaction, the product had an embryonic form of excavated rhombic dodecahedra (Figure 2a). Each particle is 10 nm in size, including a solid inner core. As the reaction time was prolonged, these NCs grew larger and larger. The average size of the ERD particles increased further to 20, 50, and 80 nm at reaction times of 3, 10, and 20 h, respectively (Figure 2b–d), while the standard $PtCu_3$ alloy phase was maintained (Figure S3). The results imply that the ERD $PtCu_3$ NCs were developed at the very beginning and then grew up during the crystal growth process. The formation mechanism of the ERD structure in our case is different from the growth–etching process found in the formation of some concave noble-metal NCs.[7]

As is well-known, for metals with an fcc structure, the {110} surface has the highest surface energy among low-index facets and is rarely exposed on surfaces.[8] Inspired by our previous results and some reports demonstrating that amine groups play an important role in controlling the surface structure of Pt nanocrystals,[1b,2e,f] we designed experiments to investigate how *n*-butylamine affect the formation of the ERD structure of $PtCu_3$ alloy NCs and tried to clarify why the {110} surfaces could be exposed. The SEM images in Figure 3 show that the morphologies of the $PtCu_3$ alloy NCs changed dramatically when the amount of *n*-butylamine used in the reaction system was adjusted (the corresponding XRD patterns are shown in Figure S4). High-magnification TEM images and the corresponding selected-area electron diffraction (SAED) patterns from different directions were also obtained to get more surface structural information (see the SI). When the amount of *n*-butylamine was decreased from 1.50 to 0.50 mL, the morphology of the as-prepared sample evolved from ERD enclosed by {110} facets (Figure 3a) to edge-concave octahedral (EC-OCT) with {111} facets exposed in the top and side areas and {110} facets in the octahedral corner area (Figure 3b). The {111} facets were confirmed by measuring the dihedral angles of neighboring {111} facets from the TEM image (Figure S5). When the volume of *n*-butylamine was further decreased to 0.30 mL, the shape of the obtained sample was also EC-OCT (Figure 3c and Figure S6), but its morphology was very close to a normal octahedron, leading to NCs with a larger surface area ratio of {111} to {110} facets. When the volume of *n*-butylamine was further reduced to 0.05 mL, the morphology became octahedral (OCT), the normal convex polyhedral shape, enclosed perfectly by eight {111}

dx.doi.org/10.1021/ja413209q | J. Am. Chem. Soc. 2014, 136, 3748–3751

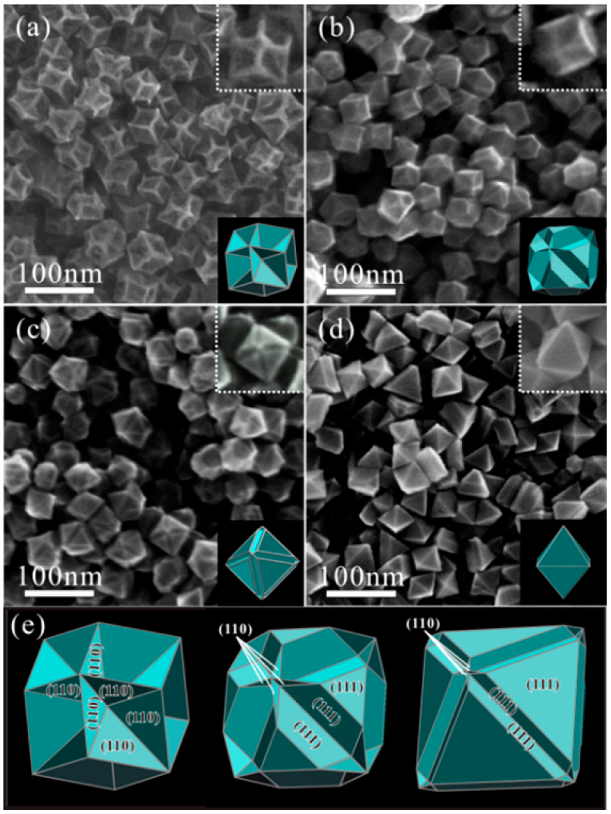

Figure 3. (a–d) SEM images and (insets) corresponding models of polyhedral $PtCu_3$ alloy NCs synthesized with different amounts of *n*-butylamine: (a) 1.50 mL, (b) 0.50 mL, (c) 0.30 mL, (d) 0.05 mL. (e) Schematic models of ERD and edge-concave octahedral (EC-OCT) shapes, showing the morphology evolution from ERD to OCT.

planes (Figure 3d and Figure S7). To more clearly show the evolution process, the magnified schematic models are shown in Figure 3e.

From the SEM images and schematic models in Figure 3, it can be concluded that the final morphology of $PtCu_3$ alloy NCs is a result of the growth competition between {110} and {111} facets at different amount of *n*-butylamine. A greater amount of *n*-butylamine leads to a greater number of exposed {110} facets in the as-prepared NCs, and a lesser amount leads to more exposed {111} facets. To explore the role of *n*-butylamine, it was substituted with other organic amines (*n*-hexylamine and *n*-octylamine). It was found the ERD $PtCu_3$ alloy NCs can be formed by other amines (Figure S8), but the shapes of the NCs are not as homogeneous as those obtained using *n*-butylamine. This result suggests that the amine group is essential to the formation of the ERD $PtCu_3$ alloy NCs. The FT-IR spectrum of the purified $PtCu_3$ ERD NCs also showed the presence of amine groups, which could be due to the adsorption of amines on the surfaces of the ERD NCs (Figure S9).

On the basis of the above results, we propose the following mechanism for the growth of the ERD structure with {110} facets. First, solid nuclei form during the nucleation stage. When *n*-butylamine is absent or its concentration is low, $PtCu_3$ alloy crystals grow in the normal way, leading to the formation of OCT particles with the most stable {111} facets (Figure 3d and Figure S7). When the concentration of *n*-butylamine is increased, the growth on the ⟨110⟩ edges of the nuclei is blocked by adsorption on the ⟨110⟩ edge sites, resulting in the formation of EC-OCT NCs (Figure 3c and Figure S6). At the same time, the {110} facets are stabilized by the adsorption of amine, which causes the formation of {110} facets in the octahedral corner area. When the amount of *n*-butylamine is increased further, the degree of truncation increases. At the same time, the number of {110} facets increases, and finally ERD NCs form. It should be pointed out that the ultrathin nanosheets with exposed {110} surfaces form in the corner area of EC-OCT particles and have the same thickness in both EC-OCT and ERD NCs. To date, we do not understand why such ultrathin nanosheets are preferred during crystal growth.

Pt-based NCs are efficient electrocatalysts for organic fuel molecules, and incorporation of 3d transition metals into Pt catalysts can improve the catalytic activity and antipoisoning activity.[9] We therefore examined the electrocatalytic performance by choosing formic acid as a target fuel molecule. For comparison, commercial Pt black was chosen as a reference catalyst. Figure 4a shows the catalytic results of as-prepared ERD

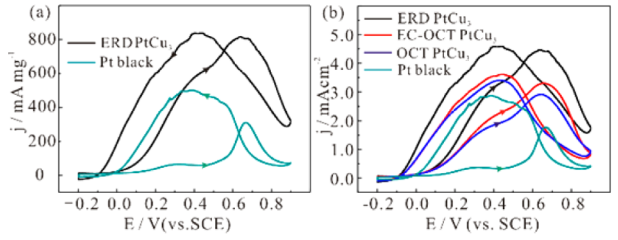

Figure 4. (a) CVs measured for the as-prepared ERD $PtCu_3$ alloy NCs and commercial Pt black in a N_2-purged 0.5 M H_2SO_4 + 0.25 M HCOOH solution. Scan rate: 50 mV s^{-1}. (b) CVs measured for three as-prepared $PtCu_3$ alloy NCs with different shapes and commercial Pt black in a N_2-purged 0.5 M H_2SO_4 + 0.25 M HCOOH solution. Scan rate: 50 mV s^{-1}.

$PtCu_3$ alloy NCs and commercial Pt black toward formic acid oxidation. The cyclic voltammograms (CVs) show that the peak current densities for formic acid oxidation at 0.65 V in the forward potential scan are 310 and 815 mA mg^{-1} for commercial Pt black and the ERD $PtCu_3$ alloy NCs, respectively, indicating the mass electrocatalytic ability of the ERD $PtCu_3$ alloy NCs is higher than that of commercial Pt black. The measured oxidation current density on ERD $PtCu_3$ alloy NCs is about 2.63 times more than the commercial Pt black. The enhanced mass catalytic activity of ERD $PtCu_3$ alloy NCs should be attributed to the high surface area and synergistic effect resulting from the alloy structure.

In addition, it is well-known that the catalytic property of bimetallic NCs also has a vital relationship with their surface structure.[10] To attain their surface-dependent catalytic activities, the catalytic properties of as-prepared samples of ERD NCs with exposed {110} facets, EC-OCT NCs enclosed by {110} and {111} facets, and OCT NCs with {111} planes were measured. For comparison, commercial Pt black was chosen as a reference material. Figure 4b shows the catalytic results for the three as-prepared $PtCu_3$ alloy NCs and commercial Pt black toward formic acid oxidation. It can be seen that the peaks for direct oxidation of formic acid to CO_2 at about 0.4 V in the forward scan correspond to current densities of 0.34, 1.85, 2.15, and 3.15 mA cm^{-2} for commercial Pt black and OCT, EC-OCT, and ERD $PtCu_3$ alloy NCs, respectively. The results indicate that the process of direct formic acid oxidation was enhanced by Cu alloying and that the electrocatalytic ability of the ERD $PtCu_3$ alloy NCs with exposed {110} facets is stronger than that of octahedra with {111} facets. The enhanced electrocatalytic

dx.doi.org/10.1021/ja413209q | J. Am. Chem. Soc. 2014, 136, 3748–3751

ability of the ERD NCs can be attributed to the high-energy surface compared with the OCT and EC-OCT NCs. In addition, it is known that the ratio of the forward oxidation current density peak (j_f) to the reverse peak (j_b) (i.e., j_f/j_b) reflects the catalyst tolerance.[11] A higher j_f/j_b indicates a better tolerance. The j_f/j_b ratio of $PtCu_3$ alloy NCs is in the range from 0.85 to 0.95, which is much higher than the value of 0.61 for Pt black. The j_f/j_b value is highest for the ERD $PtCu_3$ alloy NCs, indicating that the antipoisoning ability of the {110} facets is the highest. To further understand the excellent antipoisoning ability of ERD NCs, CO stripping was measured. It was found that the oxidation of CO on the ERD NCs is much easier than that on OCT $PtCu_3$ alloy NCs and Pt black, as the oxidation potentials of CO on the ERD NCs are negative by 50 mV and 100 mV, respectively (Figure S11). In addition to the high catalytic activity, the stability of the ERD $PtCu_3$ alloy NCs was also found to be excellent during the electrochemical measurements in comparison with the commercial Pt black catalyst (Figures S12 and S13).

In summary, we successfully synthesized ERD $PtCu_3$ alloy NCs via a coreduction method in the presence of *n*-butylamine. The ERD $PtCu_3$ alloy NCs are constructed with ultrathin nanosheets of high-energy {110} facets. We found by a series of controlled experiments that the amine is vital for the formation of the unique ERD $PtCu_3$ alloy NCs. Because of the special excavated structure, the surface area is very large (measured as 77 $m^2\ g^{-1}$ by CO stripping). The measurement of electrochemical catalytic oxidation of formic acid showed that the ERD $PtCu_3$ alloy NCs exhibit excellent electrocatalytic performance and high antipoisoning activity.

■ ASSOCIATED CONTENT

Ⓢ Supporting Information

Experimental details, additional TEM images and corresponding SAED patterns, HAADF-STEM-EDS mapping images, XRD patterns, CVs, and IR spectra. This material is available free of charge via the Internet at http://pubs.acs.org.

■ AUTHOR INFORMATION

Corresponding Author

zxxie@xmu.edu.cn

Notes

The authors declare no competing financial interest.

■ ACKNOWLEDGMENTS

This work was supported by the National Basic Research Program of China (Grants 2011CBA00508 and 2013CB933901) and the National Natural Science Foundation of China (Grants 21131005, 21333008, and J1030415).

■ REFERENCES

(1) (a) Tian, N.; Zhou, Z. Y.; Sun, S. G.; Ding, Y.; Wang, Z. L. *Science* **2007**, *316*, 732. (b) Huang, X. Q.; Zhao, Z. P.; Fan, J. M.; Tan, Y. M.; Zheng, N. F. *J. Am. Chem. Soc.* **2011**, *133*, 4718. (c) Zhang, L.; Chen, D. Q.; Jiang, Z. Y.; Zhang, J. W.; Xie, S. F.; Kuang, Q.; Xie, Z. X.; Zheng, L. S. *Nano Res.* **2012**, *5*, 181. (d) Zhou, W.; Wu, J. B.; Yang, H. *Nano Lett.* **2013**, *13*, 2870. (e) van der Vliet, D. F.; Wang, C.; Li, D. G.; Paulikas, A. P.; Greeley, J.; Rankin, R. B.; Strmcnik, D.; Tripkovic, D.; Markovic, N. M.; Stamenkovic, V. R. *Angew. Chem., Int. Ed.* **2012**, *51*, 3139.

(2) (a) Wu, Y.; Cai, S. F.; Wang, D. S.; He, W.; Li, Y. D. *J. Am. Chem. Soc.* **2012**, *134*, 8975. (b) Huang, X. Q.; Zhu, E. B.; Chen, Y.; Li, Y. J.; Chiu, C. Y.; Xu, Y. X.; Lin, Z. Y.; Duan, X. F.; Huang, Y. *Adv. Mater.* **2013**, *25*, 2974. (c) Zhang, Z. C.; Yang, Y.; Nosheen, F.; Wang, P. P.; Zhang, J. C.; Zhuang, J.; Wang, X. *Small* **2013**, *9*, 3063. (d) Zhu, H. Y.; Zhang, S.; Guo, S. J.; Su, D.; Sun, S. H. *J. Am. Chem. Soc.* **2013**, *135*, 7130. (e) Saleem, F.; Zhang, Z. C.; Xu, B.; Xu, X. B.; Wang, X. *J. Am. Chem. Soc.* **2013**, *135*, 18304. (f) Wang, S. B.; Zhu, W.; Ke, J.; Yin, A. X.; Zhang, Y. W.; Yan, C. H. *Chem. Commun.* **2013**, *49*, 7168.

(3) (a) Zhang, L.; Zhang, J. W.; Kuang, Q.; Xie, S. F.; Jiang, Z. Y.; Xie, Z. X.; Zheng, L. S. *J. Am. Chem. Soc.* **2011**, *133*, 17114. (b) Zhou, K. B.; Li, Y. D. *Angew. Chem., Int. Ed.* **2012**, *51*, 602. (c) Zhang, J. W.; Hou, C. P.; Huang, H.; Zhang, L.; Jiang, Z. Y.; Chen, G. X.; Jia, Y. Y.; Kuang, Q.; Xie, Z. X.; Zheng, L. S. *Small* **2013**, *9*, 538.

(4) (a) Xu, D.; Liu, Z. P.; Yang, H. Z.; Liu, Q. S.; Zhang, J.; Fang, J. Y.; Zou, S. Z.; Sun, K. *Angew. Chem., Int. Ed.* **2009**, *48*, 4217. (b) Jiang, Y. Q.; Jia, Y. Y.; Zhang, J. W.; Zhang, L.; Huang, H.; Xie, Z. X.; Zheng, L. S. *Chem.—Eur. J.* **2013**, *19*, 3119. (c) Liu, X. W.; Wang, D. S.; Li, Y. D. *Nano Today* **2012**, *7*, 448.

(5) (a) Yin, A. X.; Min, X. Q.; Zhu, W.; Liu, W. C.; Zhang, Y. W.; Yan, C. H. *Chem.—Eur. J.* **2012**, *18*, 777. (b) Quan, Z. W.; Wang, Y. X.; Fang, J. Y. *Acc. Chem. Res.* **2013**, *46*, 191.

(6) (a) Wu, Y.; Wang, D. S.; Niu, Z. Q.; Chen, P. C.; Zhou, G.; Li, Y. D. *Angew. Chem., Int. Ed.* **2012**, *51*, 12524. (b) Zhang, H.; Jin, M. S.; Xia, Y. N. *Angew. Chem., Int. Ed.* **2012**, *51*, 7656. (c) Xia, B. Y.; Wu, H. B.; Wang, X.; Lou, X. W. *J. Am. Chem. Soc.* **2012**, *134*, 13934.

(7) Liu, M. C.; Zheng, Y. Q.; Zhang, L.; Guo, L. J.; Xia, Y. N. *J. Am. Chem. Soc.* **2013**, *135*, 11752.

(8) (a) Lin, H. X.; Lei, Z. C.; Jiang, Z. Y.; Hou, C. P.; Liu, D. Y.; Xu, M. M.; Tian, Z. Q.; Xie, Z. X. *J. Am. Chem. Soc.* **2013**, *135*, 9311. (b) Zhang, Z. C.; Hui, J. F.; Liu, Z. C.; Wang, X.; Zhuang, J.; Wang, X. *Langmuir* **2012**, *28*, 14845.

(9) (a) Wu, Y.; Wang, D. S.; Chen, X. B.; Zhou, G.; Yu, R.; Li, Y. D. *J. Am. Chem. Soc.* **2013**, *135*, 12220. (b) Liu, X. J.; Cui, C. H.; Gong, M.; Li, H. H.; Xue, Y.; Fan, F. J.; Yu, S. H. *Chem. Commun.* **2013**, *49*, 8704. (c) Liu, X. W.; Wang, W. Y.; Li, H.; Li, L. S.; Zhou, G. B.; Yu, R.; Wang, D. S.; Li, Y. D. *Sci. Rep.* **2013**, *3*, 1404. (d) Carpenter, M. K.; Moylan, T. E.; Kukreja, R. S.; Atwan, M. H.; Tessema, M. M. *J. Am. Chem. Soc.* **2012**, *134*, 8535. (e) Strasser, P.; Koh, S.; Anniyev, T.; Greeley, J.; More, K.; Yu, C. F.; Liu, Z. C.; Kaya, S.; Nordlund, D.; Ogasawara, H.; Toney, M. F.; Nilsso, A. *Nat. Chem.* **2010**, *2*, 454.

(10) (a) Lee, Y. W.; Kim, D. H.; Hong, J. W.; Kang, S. W.; Lee, S. B.; Han, S. W. *Small* **2013**, *9*, 660. (b) Yin, A. X.; Min, X. Q.; Zhang, Y. W.; Yan, C. H. *J. Am. Chem. Soc.* **2011**, *133*, 3816. (c) Wu, J. B.; Yang, H. *Acc. Chem. Res.* **2013**, *46*, 1848. (d) Wang, D. S.; Li, Y. D. *Adv. Mater.* **2011**, *23*, 1044. (e) Zhang, L.; Niu, W. X.; Xu, G. B. *Nano Today* **2012**, *7*, 586.

(11) (a) Guo, S. J.; Fang, Y. X.; Dong, S. J.; Wang, E. K. *J. Phys. Chem. C* **2007**, *111*, 17104. (b) Guo, S. J.; Dong, S. J.; Wang, E. K. *Chem.—Eur. J.* **2008**, *14*, 4689.